Journal of Solid State Chemistry 181 (2008) 2989–2993

Contents lists available at ScienceDirect

Journal of Solid State Chemistry

journal homepage: www.elsevier.com/locate/jssc

Interatomic versus intraatomic Ru interactions in perovskites

Sangwon Kim, Ronald I. Dass, John B. Goodenough *

Texas Materials Institute, The University of Texas at Austin, ETC 9.102, Austin, TX 78712, USA

ARTICLE INFO

Article history:
Received 28 May 2008
Received in revised form
13 July 2008
Accepted 15 July 2008
Available online 24 July 2008

Keywords:
Magnetic properties
Spin–orbit coupling
Griffiths phase
Double perovskites

ABSTRACT

The competition between interatomic Ru–O–Ru interactions responsible for itinerant-electron ferromagnetism in $SrRuO_3$ and intraatomic spin–orbit coupling that suppresses some Ru–O–Ru magnetic interactions in $CaRuO_3$ so as to prevent long-range magnetic order has been further tested by investigating the double perovskites La_2RuZnO_6, La_2RuCoO_6, La_2TiCoO_6, and the solid solution $Ca_{2-2x}La_{2x}Ru_{2-x}Co_xO_6$ ($0.0 \leqslant x \leqslant 1.0$). The paramagnetic state of the low-spin, localized Ru^{4+}:t^4e^0 configuration of $LaRuZnO_6$ undergoes a progressive transition on lowering the temperature to a non-magnetic state ($J=0$) as a result of spin–orbit coupling, $\lambda \mathbf{L}\cdot\mathbf{S}$. Comparison of the susceptibilities of La_2RuCoO_6 and La_2TiCoO_6 shows a similar behavior with long-range antiferromagnetic cobalt ordering via non-magnetic $RuO_{6/2}$ and $TiO_{6/2}$ bridges. Comparison is also made of the effect of substituting Ga for Ru in $CaRuO_3$ with the effect of other dopants M in $CaRu_{1-x}M_xO_3$. The evolution of transport properties in $Ca_{2-2x}La_{2x}Ru_{2-x}Co_xO_6$ is also presented.

1. Introduction

In 1966, Callaghan et al. [1] first reported that metallic $SrRuO_3$ is a ferromagnetic perovskite with a Curie temperature $T_C \approx 160$ K. The 4*d* electrons of the low-spin Ru^{4+} ions occupy a narrow π^* band that is two-thirds filled, but the spontaneous magnetization extrapolated to $T=0$ K is $M_s(0)=1.4\,\mu_B$/Ru [2], which is reduced from the spin-only value of $2.0\,\mu_B$/Ru. Broadening the π^* band by substituting the more basic Ba^{2+} ion for Sr^{2+} ion in the cubic-perovskite phase obtained by high-pressure synthesis lowers both T_C and $M_s(0)$ as anticipated for itinerant-electron ferromagnetism [3]. Substitution of the more acidic Ca^{2+} ion for Sr^{2+} narrows the π^* band, but this band narrowing does not lead to an increase in the $M_s(0)$ for any value of *x* in the system $Sr_{1-x}Ca_xRuO_3$; rather a Griffiths phase [4] is found in which both T_C and the volume fraction of long-range ferromagnetic order decrease with increasing *x* [3]. Although $CaRuO_3$ is metallic like $SrRuO_3$, there is no long-range magnetic order in its RuO_3 array [5]. At high temperatures, the paramagnetic susceptibility exhibits a Curie–Weiss behavior with a μ_{eff} that changes little with *x*, but the Weiss constant becomes $\theta_W < T_C$ and $(T_C - \theta_W)$ increases with *x* until T_C vanishes for $x > 0.6$ and a $\theta_W < 0$ is found [6]. Nevertheless, even though a $\theta_W < 0$ is found in $CaRuO_3$, there is no evidence that the Ru–O–Ru interactions have changed sign. He and Cava [7] have reported that substitution of non-magnetic Ti^{4+} for Ru^{4+} in $CaRu_{1-x}M_xO_3$ induces long-range ferromagnetic order over a wide range of *x*, and NMR data of Daniel et al. [8] as well as zero-field μSR measurements of Uemura et al. [9] have provided evidence of ferromagnetic fluctuations in low-temperature $CaRuO_3$. Clearly the π^* electrons of $CaRuO_3$ approach the transition from itinerant- to localized-electron behavior from the itinerant-electron side, and it is therefore of interest to explore further the role of the intraatomic spin–orbit coupling that competes with the interatomic interactions responsible for the itinerant-electron behavior.

In the double perovskites $La_2Ru^{4+}M^{2+}O_6$, the Ru^{4+} and M^{2+} ions order into alternate octahedral sites. In these oxides, the Ru^{4+}-ion 4*d*-electron configuration should be localized. Bos et al. [10] have shown that the Co^{2+} spins of La_2RuCoO_6 order antiferromagnetically below $T_N = 25$ K, but they were unable to detect any magnetic moment on the Ru^{4+} ions despite the observation of a Ru^{4+}-ion contribution to the paramagnetic susceptibility at high temperatures. This behavior may be explained by a spin–orbit coupling that is active at low temperatures since the ground state $^3T_{1g}$ would then have a principal quantum number $J=0$ [11]; the Co^{2+} ions would then couple antiferromagnetically across a non-magnetic $RuO_{6/2}$ complex as across a $TiO_{6/2}$ complex.

In order to probe further the role of spin–orbit coupling on the Ru^{4+} ions, we have compared the magnetic properties of La_2RuZnO_6 and La_2TiCoO_6 with those of La_2RuCoO_6. Our results show that at low temperatures, the ground state of the localized-electron Ru^{4+} configuration has $J=0$ as a result of spin–orbit coupling provided local site distortions do not suppress the orbital angular momentum; but at higher temperatures, excitations to states with a magnetic moment contribute to a μ_{eff}. We have also investigated the nominal system $Ca_{2-2x}La_{2x}Ru_{2-x}Co_xO_6$

* Corresponding author.
E-mail addresses: jgoodenough@mail.utexas.edu, costa97@gmail.com (J.B. Goodenough).

0022-4596/$ - see front matter © 2008 Elsevier Inc. All rights reserved.
doi:10.1016/j.jssc.2008.07.023

($0.0 \leqslant x \leqslant 1.0$) where we have attempted to retain low-spin Ru^{4+} ions and high-spin Co^{2+} ions; our data show evidence of a weak first-order crossover from itinerant- to localized-electron behavior on at least some Ru^{4+} ions near $x \approx 0.2$ with the appearance of long-range antiferromagnetic order in the range $0.4 \leqslant x \leqslant 0.9$ providing evidence that the $4d^4$ configuration is not localized ($J = 0$) on all the Ru^{4+} ions in the atomically disordered samples. Since Ru volatilization during preparation introduces some Ru^{5+}/Ru^{4+} mixed valence, we have prepared $CaRu_{0.9}Ga_{0.1}O_3$ to determine the effect of a mixed Ru^{5+}/Ru^{4+} valence in the absence of a partially occupied d shell to confirm that a mixed Ru^{5+}/Ru^{4+} valence alone does not induce long-range magnetic order where the spin–orbit coupling is not suppressed.

2. Experimental procedures

La_2RuZnO_6 and La_2TiCoO_6 were prepared by solid-state reaction of stoichiometric amounts of La_2O_3, RuO_2, ZnO_3, TiO_2, and Co_3O_4. TGA (Perkin-Elmer TGA7 system) was conducted on the La_2O_3 powder from room temperature to 950 °C to estimate the true weight. An excessive amount of ZnO (2%) was added to compensate for Zn evaporation, and the TiO_2, was precalcined at 900 °C for 12 h. La_2RuZnO_6 was fired three times at 800 °C for 12 h and once at 1025 °C for 12 h in air with intermediate grinding. La_2TiCoO_6 was fired at 800, 1000, and 1150 °C for 12 h each in air. The samples were cold-pressed and fired at 1025 and 1250 °C, respectively, for 24 h in air before measurement.

The system $Ca_{2-2x}La_{2x}Ru_{2-x}Co_xO_6$ ($0.0 \leqslant x \leqslant 1.0$) and the compounds $Ca_{1.8}La_{0.2}Ru_{1.9}Ni_{0.1}O_6$ and $CaRu_{0.9}Ga_{0.1}O_3$ were all prepared by the "polymerizable-complex method" (PCM) [12]. The complexes used were $Ca(NO_3)_2 \cdot xH_2O$, $La(NO_3)_3 \cdot xH_2O$, $RuCl_3 \cdot xH_2O$, $Co(NO_3)_2 \cdot xH_2O$, $Ni(CH_3COO)_2 \cdot xH_2O$, and $Ga(NO_3)_3 \cdot xH_2O$. To find the exact value of the water of crystallization in these precursors, a TGA from 20 to 1000 °C was made in a reducing environment. The X-ray diffraction results showed the remaining compounds were CaO, La_2O_3, Ru, Co, Ni, and Ga_2O_3. Stoichiometric amounts of the metal nitrates were dissolved in deionized water (H_2O), and citric acid was added as a chelating agent to this solution. Then, ethylene glycol was added for the polyesterification while heating the solution [13]. After the resin was well-ground, each sample was first fired at 400 °C for 24 h in air, 3 times at 800 °C for 12 h, and then 3 times at 1150 °C for 6 h with a cooling rate of 6 °C/h. Finally, the sample was cold-pressed and fired at 1150 °C for 6 h. As much as 20 ton was applied to reduce porosity and to reduce the grain-forming temperature of the sample.

The phases of the samples were analyzed with a Philips PW 1729 powder X-ray diffractometer and PW3040 XPERT equipped with monochromator and Cu $K\alpha$ radiation (1.54059 Å) over the range of $10^\circ \leqslant 2\theta \leqslant 90^\circ$ at room temperature. The results were refined with the program JADE. The resistivity of the samples was measured with a four-probe technique on the pressed pellets over the temperature interval $7\,K \leqslant T \leqslant 300\,K$. A laboratory-built apparatus was used to measure the thermoelectric power of the samples over the range $20\,K \leqslant T \leqslant 300\,K$. Finally, a superconducting quantum interference device (SQUID) was used to obtain the magnetic susceptibility and to check for any thermal hysteresis of samples over the range $5\,K \leqslant T \leqslant 300\,K$.

3. Results

The X-ray diffraction results for $Ca_{2-2x}La_{2x}Ru_{2-x}Co_xO_6$ ($0.0 \leqslant x \leqslant 1.0$) were first refined with the orthorhombic crystal symmetry *Pnma* and the monoclinic $P2_1/n$; the samples for $x \leqslant 0.8$ were found to maintain *Pnma* while the rest ($x \geqslant 0.9$) favors the $P2_1/n$ symmetry for ordering of the Ru^{4+} and Co^{2+} ions. The lattice parameters, Table 1, increase nearly linearly with x. This increase reflects the substitution of the larger ions Co^{2+} (0.735 Å) and La^{3+} (1.20 Å) for Ru^{4+} (0.620 Å) and Ca^{2+} (1.18 Å), respectively. However, Fig. 1 shows a small, but fairly abrupt change in the unit-cell volume between $x = 0.1$ and 0.2. Scanning electron microscopy energy dispersive spectroscopy (SEM EDS) measurements were conducted on these samples to confirm the cation stoichiometry. These measurements confirmed there was no discontinuity in the loss of Ru between $x = 0.1$ and 0.2. Due to the facile volatilization of Ru above 600 °C, the presence of some Ru vacancies was found inevitable. Bos and Attfield [14] used X-ray absorption near-edge structure (XANES) spectroscopy to verify that the Ru^{5+}/Ru^{4+} redox couple is located higher than the Co^{3+}/Co^{2+} redox couple. Therefore, the presence of Ru vacancies leads to the formation of Ru^{5+} ions in the system. Samples were chosen randomly to find the oxygen contents, and TGA results confirmed that most were nearly oxygen stoichiometric (Table 1). $CaRu_{0.9}Ga_{0.1}O_3$ and $Ca_{1.8}La_{0.2}Ru_{1.9}Ni_{0.1}O_6$ had *Pnma* crystal symmetry while La_2RuZnO_6 and La_2TiCoO_6 were monoclinic $P2_1/n$.

Fig. 2 shows that the electrical resistivity $\rho(T)$ of $CaRuO_3$ exhibits a bad-metal behavior. However, $Ca_{2-2x}La_{2x}Ru_{2-x}Co_xO_6$ undergoes a smooth transition to a semiconductive temperature dependence at $x \approx 0.1$. The $\rho(T)$ for $x \approx 1.0$ was fitted to a Variable Range Hopping equation with a temperature-dependent prefactor

$$\rho = \rho_0 \left(\frac{T}{T_0}\right)^{1/2} \exp\left(\left(\frac{T_0}{T}\right)^{1/4}\right) \quad (1)$$

as originally proposed by Bos and Attfield [14]; Kim and Battle [15] used the same equation to fit the $\rho(T)$ curves for Sr_2RuCoO_6, Ba_2RuCoO_6, $LaSrRuCoO_6$, and $LaBaRuCoO_6$.

Fig. 3 shows that the thermoelectric power $\alpha(T)$ for all samples remains positive. A kink in $\alpha(T)$ at low temperature for $x = 0.0$ may signal the presence of a phonon-drag component; the samples for $x \geqslant 0.1$ do not show such a behavior, as is shown in the inset of Fig. 3. A higher $\alpha(300\,K)$ for $x = 1.0$ shows that this sample is more nearly stoichiometric.

According to Fig. 4, the system goes through long-range antiferromagnetic ordering with $22\,K \leqslant T_N \leqslant 32\,K$ for $x \geqslant 0.4$ while samples with $x \leqslant 0.3$ lack any long-range magnetic ordering. The inset in Fig. 4 shows a steady increase in T_N until the system changes crystal symmetry from *Pnma* to $P2_1/n$; a $T_N \approx 26\,K$ for the $x = 1.0$ sample agrees with previous results [14,16]. As shown in Fig. 5, long-range magnetic ordering is also absent in $CaRu_{0.9}Ga_{0.1}O_3$ in agreement with Hardy et al. [17]; this result confirms that the effect of mixed valence alone is not strong enough to induce a spontaneous magnetization in $CaRu_{1-x}M_xO_3$. Ni substitution, instead of Co, also fails to induce any noticeable long-range ordering in $Ca_{1.8}La_{0.2}Ru_{1.9}Ni_{0.1}O_6$. The $1/\chi(T)$ for La_2RuZnO_6, shown in the inset of Fig. 5, was found to have the same character as that of $CaRuO_3$. Long-range antiferromagnetic ordering in La_2TiCoO_6 at a $T_N \approx 16\,K$ (Fig. 6) is in agreement with a previous report [18]; the $1/\chi(T)$ curve for La_2RuCoO_6 shows no thermal hysteresis below 170 K, which confirms the antiferromagnetic transition for La_2RuCoO_6 is second order. Similarly, no sign of thermal hysteresis was found near T_N in La_2TiCoO_6.

The slopes of the paramagnetic $1/\chi(T)$ curves for the system $Ca_{2-2x}La_{2x}Ru_{2-x}Co_xO_6$ are not constant below 300 K. This fact, noted by Yoshimura et al. [19] for $x = 0$, was emphasized by Jin et al. [3] to be due to the progressive onset of spin–orbit coupling with lowering temperature and the appearance of a Griffiths phase in $Sr_{1-x}Ca_xRuO_3$.

Table 1
The room-temperature structural properties and oxygen content $(6-\delta)$ in $Ca_{2-2x}La_{2x}Ru_{2-x}Co_xO_{6-\delta}$ $(0.0 \leqslant x \leqslant 1.0)$, $CaRu_{0.9}Ga_{0.1}O_3$, $Ca_{1.8}La_{0.2}Ru_{1.9}Ni_{0.1}O_6$, La_2RuZnO_6, and La_2TiCoO_6

x	Space group	a (Å)	b (Å)	c (Å)	θ (Å)	V (Å^3)	O content $(6-\delta)$
0.0	*Pnma*	5.527 (1)	7.657 (1)	5.351 (1)	90	226.45 (11)	5.99 (1)
0.1	*Pnma*	5.538 (1)	7.678 (1)	5.373 (1)	90	228.47 (11)	5.98 (1)
0.2	*Pnma*	5.545 (2)	7.723 (1)	5.410 (1)	90	231.68 (15)	–
0.3	*Pnma*	5.556 (2)	7.754 (2)	5.439 (3)	90	234.37 (28)	–
0.4	*Pnma*	5.560 (2)	7.768 (3)	5.463 (3)	90	235.99 (30)	5.93 (2)
0.5	*Pnma*	5.580 (4)	7.797 (4)	5.483 (5)	90	238.56 (51)	–
0.6	*Pnma*	5.594 (1)	7.817 (2)	5.506 (2)	90	240.77 (16)	5.98 (2)
0.7	*Pnma*	5.606 (1)	7.840 (1)	5.534 (1)	90	243.24 (12)	–
0.8	*Pnma*	5.622 (1)	7.854 (1)	5.544 (1)	90	244.79 (11)	–
0.9	$P2_1/n$	5.627 (1)	7.867 (1)	5.562 (1)	90.07 (1)	246.20 (11)	–
1.0	$P2_1/n$	5.638 (1)	7.878 (1)	5.574 (1)	90.08 (1)	247.56 (11)	6.01 (3)
$CaRu_{0.9}Ga_{0.1}O_3$	*Pnma*	5.507 (1)	7.650 (1)	5.361 (1)	90	225.85 (11)	–
$Ca_{1.8}La_{0.2}Ru_{1.9}Ni_{0.1}O_3$	*Pnma*	5.533 (1)	7.681 (1)	5.360 (1)	90	227.79 (11)	–
La_2RuZnO_6	$P2_1/n$	5.684 (1)	7.901 (2)	5.586 (1)	90.06 (1)	250.86 (16)	–
La_2TiCoO_6	$P2_1/n$	5.559 (1)	5.570 (1)	7.839 (1)	89.90 (1)	242.72 (11)	–

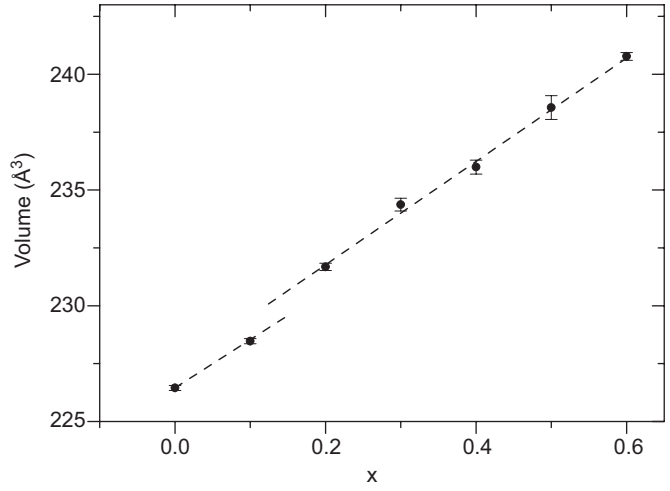

Fig. 1. The variation with x of the room-temperature cell volume for the orthorhombic compositions of the system $Ca_{2-2x}La_{2x}Ru_{2-x}Co_xO_6$ $(0.0 \leqslant x \leqslant 0.6)$.

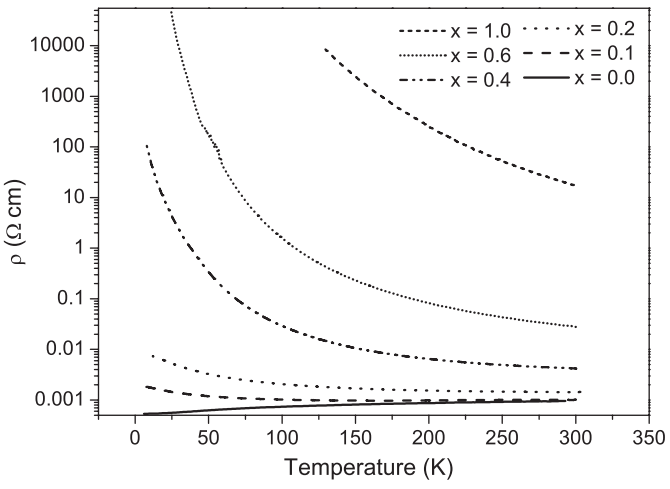

Fig. 2. The variation with temperature of the electrical resistivity $\rho(T)$ for compositions in the system $Ca_{2-2x}La_{2x}Ru_{2-x}Co_xO_6$ ($x = 0.0$, 0.1, 0.2, 0.4, 0.6, 1.0).

4. Discussion

In the double-perovskite phases $La_2RuM^{2+}O_6$, all the 4*d* electrons of the Ru^{4+} ions should be localized for ideal cation ordering since the Ru^{4+} ions would then interact with one another only through Ru–O–M–O–Ru linkages. However, even a fully ordered sample will contain antiphase boundaries across which are Ru–O–Ru interactions. Even if these interactions do not give rise to itinerant-electron behavior with magnetic moments at low temperature, the presence of Ru^{5+} ions will introduce spins stable to lowest temperatures. Although these spins mask any characteristic suppression of the Ru^{4+}-ion moments at low temperatures due to spin–orbit coupling, nevertheless Fig. 5 shows a curvature of the $1/\chi(T)$ curve of nominal La_2RuZnO_6 similar to that

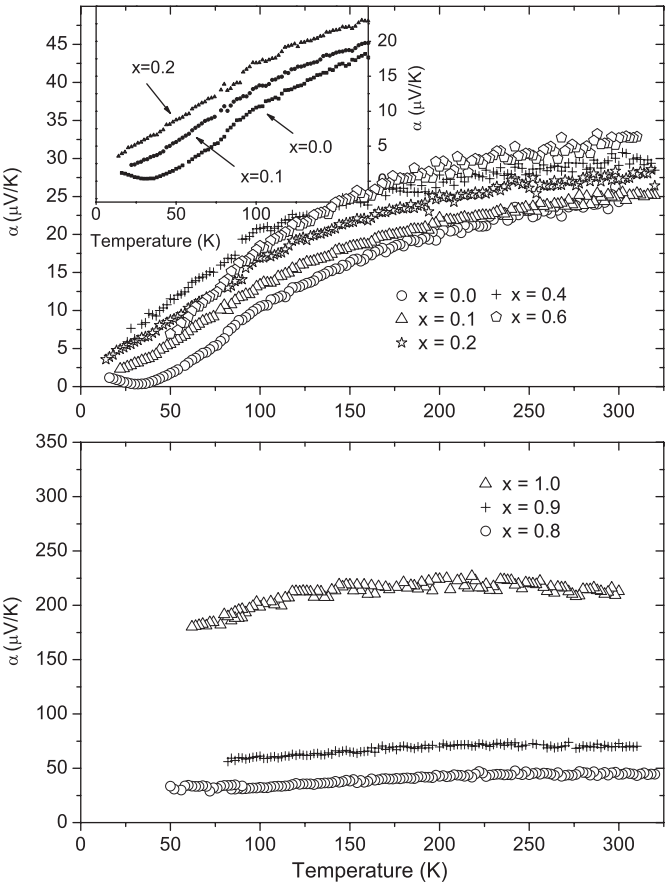

Fig. 3. The variation with temperature of the thermoelectric power $\alpha(T)$ for compositions in the system $Ca_{2-2x}La_{2x}Ru_{2-x}Co_xO_6$ $(0.0 \leqslant x \leqslant 1.0)$. The inset shows the behavior in some of the compositions for $T < 200$ K $(0.0 \leqslant x \leqslant 0.2)$.

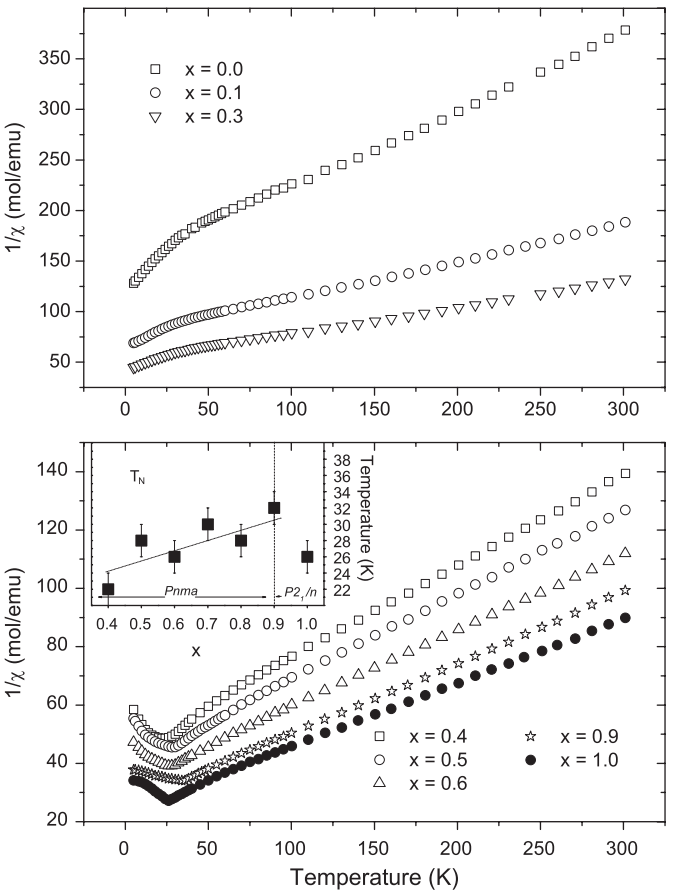

Fig. 4. The temperature dependence of the inverse magnetic susceptibility $1/\chi(T)$ under an applied magnetic field $H = 500$ Oe for different compositions in the system for $Ca_{2-2x}La_{2x}Ru_{2-x}Co_xO_6$. The inset shows the variation of the Néel temperature T_N with x for $x \geq 0.4$ (ZFC-FW).

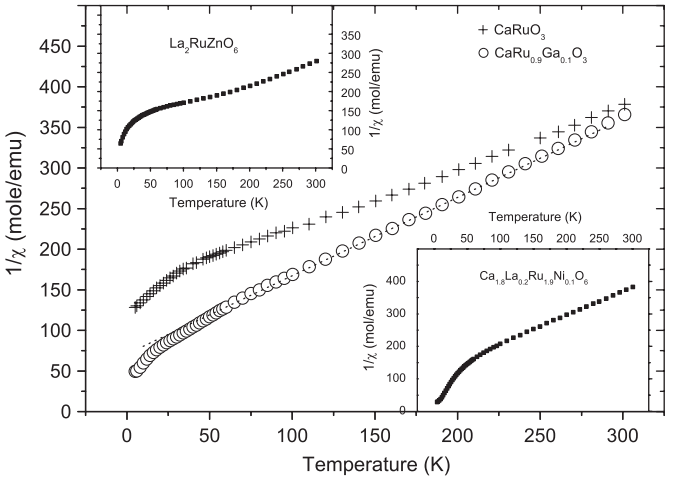

Fig. 5. The temperature dependence of the inverse magnetic susceptibility $1/\chi(T)$ under an applied magnetic field $H = 500$ Oe for $CaRuO_3$ and $CaRu_{0.9}Ga_{0.1}O_3$ (ZFC-FW). The inset shows the behavior in La_2RuZnO_6 and $Ca_{1.8}La_{0.2}Ru_{1.9}Ni_{0.1}O_6$.

with $CaRuO_3$; it is characteristic of a progressive suppression of spin–spin interactions as temperature decreases, and there is no evidence of any long-range magnetic order of Ru^{4+}-ion spins in La_2RuZnO_6, which is consistent with a $J = 0$ ground state on the Ru^{4+} ions. Moreover, antiferromagnetic order at $T_N \approx 16$ K (or 21 K according to Ref. [20]) in La_2TiCoO_6 is similar to the $T_N = 25$ K

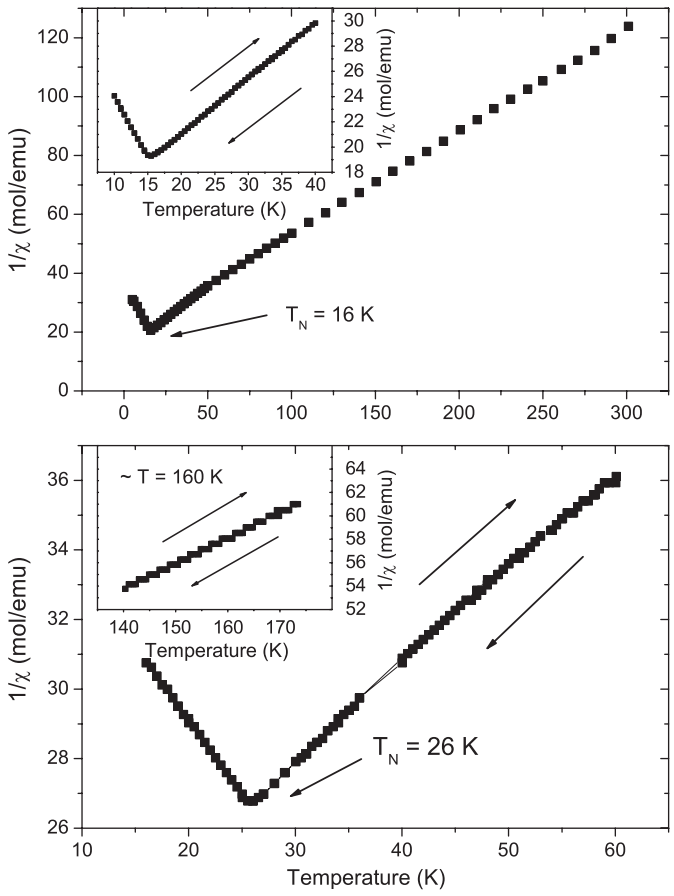

Fig. 6. (a) The temperature dependence of the inverse magnetic susceptibility $1/\chi(T)$ under an applied magnetic field $H = 1000$ Oe for La_2TiCoO_6 (FC-FW). The inset shows a lack of thermal hysteresis in La_2TiCoO_6. (b) The $1/\chi(T)$ for La_2RuCoO_6 shows a lack of thermal hysteresis (FC-FW) around $T = 160$ K and $T_N = 26$ K.

found in La_2RuCoO_6; the $RuO_{6/2}$ bridges between Co^{2+} ions appear to provide a similar magnetic coupling between the Co^{2+} ions, which is consistent with a $J = 0$ at low temperatures for the $RuO_{6/2}$ bridge.

The Ru^{4+}–O^{2-}–Ru^{4+} interactions in the $A^{2+}RuO_3$ perovskites provide a narrow π^* band at the threshold of a transition from itinerant- to localized-electronic behavior. Introduction of the aliovalent La^{3+} and Ca^{2+} ions in $Ca_{2-2x}La_{2x}Ru_{2-x}Co_xO_6$ was designed to keep the Ru^{4+} valence state, but to narrow further the π^* band of $CaRuO_3$. Unfortunately, the loss of some Ru during sample preparation drops the Fermi energy E_F into the Ru^{5+}/Ru^{4+} redox couple. Electrons in the mixed-valent Ru^{5+}/Ru^{4+} redox couple may remain itinerant even if strong correlations split this redox couple from the Ru^{4+}/Ru^{3+} redox couple. However, cation vacancies and the aliovalent La^{3+} and Co^{2+} ions perturb the periodic potential to introduce Anderson [21] localized states above a mobility edge E_C at the top of the Ru^{5+}/Ru^{4+} band. As x increases, a drop of E_C to below E_F of the conductive π^* band and correlation splitting of the Ru^{5+}/Ru^{4+} and Ru^{4+}/Ru^{3+} redox couples are both occurring. The apparent small jump in volume in the interval $0.1 < x < 0.2$ may reflect an increase in the concentration of localized $4d^4$ configurations as E_F crosses E_C and/or the π^* band of $CaRuO_3$ becomes globally split by strong electron correlations. The equilibrium average M–O bond length for localized electrons is larger than that for itinerant electrons [22]. In the range $0 \leqslant x \leqslant 0.1$, the transport data are consistent with E_C above E_F in an itinerant-electron band. Retention of the positive sign of $\alpha(T)$ as x increases is due to the presence of holes in the Ru^{5+}/Ru^{4+} redox couple.

The slope of $\alpha(T)$ in the interval $0 \leqslant x \leqslant 0.7$ does not fit a polaronic description; polaronic conduction dominates only for $0.8 \leqslant x \leqslant 1.0$.

Three features are of interest in the $Ca_{2-2x}La_{2x}Ru_{2-x}Co_xO_6$ system. First, the introduction of a Co^{2+} ion in the presence of Ru^{4+} does not induce ferromagnetic order in the Ru^{4+} array as was found with Ti^{4+} in $CaRu_{1-x}Ti_xO_3$ [7]. Second, electrostatic forces between Co^{2+} ions minimize the concentration of antiferromagnetic Co–O–Co interactions, and a $T_N \approx 25$ K appearing for $x \geqslant 0.4$ reflects regions containing a dominance of antiferromagnetic Co–O–Ru–O–Co interactions. The formation of ordered-cation regions would result in Ru-rich regions containing Ru–O–Ru bonding that are responsible for retention of a dominant itinerant-electron transport term in the thermoelectric power. Third, in the monoclinic compositional range $0.9 \leqslant x \leqslant 1.0$, long-range ordering of the Co^{2+} and Ru^{4+} ions reduces sharply the concentration of Ru–O–Ru interactions, and the transition to a $J = 0$ state at the isolated Ru^{4+} ions appears to progress below 250 K.

Finally, we ask why some atoms M substituted for Ru in $CaRu_{1-x}M_xO_3$ induce long-range ferromagnetic order while others do not. Since broadening the π^* band in $Ca_{1-y}Sr_yRuO_3$ introduces long-range ferromagnetic order, we may anticipate that M-atom substitutions that broaden the π^* band and/or suppress the orbital angular momentum may also induce long-range ferromagnetic order. For example, Ti^{4+} has a little larger ionic radius than Ru^{4+} as well as a Ti^{4+}/Ti^{3+} redox couple that lies close to the Ru^{5+}/Ru^{4+} couple. Therefore, Ti substitution for Ru in $CaRu_{1-x}Ti_xO_3$ can be expected to broaden the π^* band and to weaken the orbital angular momenta on neighboring Ru^{4+} ions. On the other hand, although Sn^{4+} has empty electronic states at energies similar to those of Ti^{4+}, the symmetry of the 5*s* orbitals is incompatible with overlap of the Ru–t orbitals in a 180° Sn–O–Ru bond; therefore, Sn^{4+} ions are not quite able to induce long-range ferromagnetic order on the Ru^{4+} ions. A trivalent cation with half-filled t^3 orbitals (e.g. Cr^{3+}, Mn^{3+}, Fe^{3+}) attracts the holes it introduces into the π^* band to give an antiferromagnetic M^{3+}–Ru^{5+} interaction that stabilizes ferrimagnetic clusters as has been shown by Maignan et al. [23]. The Ga^{3+} ion introduces mobile holes into the π^* bands; these holes become trapped by Ga^{3+} ions without becoming localized as a Ru^{5+} ion coupling antiferromagnetically to a localized spin on the Ga^{3+}.

5. Conclusions

Where the 4*d*-electron configuration is localized on an octahedral-site Ru^{4+} ion, as is the case in the double perovskites $La_2RuM^{2+}O_6$, spin–orbit coupling makes the $^3Ti_{1g}$ ground state have a principal quantum number $J = 0$. This situation allows the ion to contribute to the paramagnetic susceptibility at higher temperatures, but suppression of the ionic magnetic moment sets in below about 250 K due to the spin–orbit coupling.

The $ARuO_3$ perovskites formally containing Ru^{4+} ions exhibit unusual physical properties because the Ru–O–Ru interactions between 4*d* electrons create a narrow π^* band at the crossover from itinerant- to localized-electronic behavior and the orbital angular momentum is not fully quenched by the ligand-field splitting of π- and σ-bond orbitals. In the $Sr_{1-x}Ba_xRuO_3$ cubic-perovskite system, the electrons of the narrow π^* band give rise to an itinerant-electron ferromagnetism. However, narrowing of the π^* band in the $Sr_{1-x}Ca_xRuO_3$ system breaks the magnetic interactions between some of the Ru atoms to give rise to a Griffiths phase and finally, in $CaRuO_3$, to no long-range ferromagnetic order. Since $CaRuO_3$ remains metallic, it is not clear whether the Ru–O–Ru interactions are interrupted in the neighborhood of the Ca^{2+} ions by localized-electron fluctuations or by an entanglement of interactions between spins and orbital angular momenta. Although the effect of substituting M atoms for Ru in $CaRu_{1-x}M_xO_3$ can be rationalized qualitatively, these experiments do not clarify the origin of the suppression of the Ru–O–Ru magnetic interactions in $CaRuO_3$. They do show, however, that this suppression is not due to a competition between ferromagnetic and antiferromagnetic interactions.

Acknowledgments

We thank the Robert A. Welch Foundation of Houston, TX (Grant no. F-1066), the NSF, and the Ministry of Information and Communication (Republic of Korea) for financial support.

References

[1] A. Callaghan, C.W. Moeller, R. Ward, Inorg. Chem. 5 (1966) 1572.
[2] G. Cao, S. McCall, M. Sheppard, J.E. Crow, R.P. Guertin, Phys. Rev. B 56 (1997) 321.
[3] C.-Q. Jin, J.-S. Zhou, J.B. Goodenough, Q.Q. Liu, J.G. Zhao, L.X. Yang, Y. Yu, R.C. Yu, T. Katsura, A. Shatskiy, E. Ito, Proc. Natl. Acad. Sci. 105 (2008) 7115.
[4] R.B. Griffiths, Phys. Rev. Lett. 23 (1969) 17.
[5] T.C. Gibb, R. Greatrex, N.N. Greenwood, P. Kaspi, J. Chem. Soc. Dalton Trans. 12 (1973) 1253.
[6] J.M. Longo, P.M. Raccah, J.B. Goodenough, J. Appl. Phys. 39 (1968) 1327.
[7] T. He, R.J. Cava, J. Phys.: Condens. Matter 13 (2001) 8347; R.J. Cava, Phys. Rev. B 63 (2001) 172403.
[8] M. Daniel, J.I. Budnick, W.A. Hines, Y.D. Zhang, W.G. Clark, A.R. Moodenbaugh, J. Phys.: Condens. Matter 12 (2000) 3857.
[9] Y.J. Uemura, T. Goko, I.M. Gat-Malureanu, J.P. Carlo, P.L. Russo, A.T. Savici, A. Aczel, G.J. MacDougall, J.A. Rodriguez, G.M. Luke, S.R. Dunsiger, A. McCollam, J. Arai, C.H. Pfleiderer, P. Böni, K. Yoshimura, E. Baggio-Saitovitch, M.B. Fontes, J. Larrea, Y.V. Sushko, J. Sereni, Nat. Phys. 3 (2007) 29.
[10] J.W.G. Bos, J.P. Attfield, T.S. Chan, R.S. Liu, L.Y. Jang, Phys. Rev. B 72 (2005) 014101.
[11] J.S. Griffith, The Theory of Transition-Metal Ions, Cambridge, UK, 1961.
[12] H. M. Reichenbach, Studies of the combinatorial synthesis of catalyst oxide powders, Ph.D. Dissertation, Department of Chemical Engineer, Notre Dame, 2002.
[13] S. Sakka, Handbook of Sol–Gel Science and Technology: Processing, Characterization, and Applications, Springer, Berlin, 2004.
[14] J.W.G. Bos, J.P. Attfield, J. Mater. Chem. 15 (2005) 715.
[15] S.H. Kim, P.D. Battle, J. Solid State Chem. 114 (1995) 174.
[16] R.I. Dass, J.-Q. Yan, J.B. Goodenough, Phys. Rev. B 69 (2004) 094416.
[17] V. Hardy, B. Raveau, R. Retoux, N. Barrier, A. Maignan, Phys. Rev. B 73 (2006) 094418.
[18] K.L. Holman, Q. Huang, T. Klimczuk, K. Trzebiatowski, J.W.G. Bos, E. Morosan, J.W. Lynn, R.J. Cava, J. Solid State Chem. 180 (2007) 75.
[19] K. Yoshimura, T. Imai, T. Kiyama, K.R. Thurber, A.W. Hunt, K. Kosuge, Phys. Rev. Lett. 83 (1999) 4397.
[20] E. Rodríguez, M.L. López, J. Campo, M.L. Veiga, C. Pico, J. Mater. Chem. 12 (2002) 2798.
[21] P.W. Anderson, Phys. Rev. 109 (1958) 1492.
[22] J.B. Goodenough, Struct. Bonding 98 (2001) 1.
[23] A. Maignan, B. Raveau, V. Hardy, N. Barrier, R. Retoux, Phys. Rev. B 74 (2006) 024410.